Orbital-Specific Analysis of CO Chemisorption on Transition-Metal Surfaces

Sara E. Mason,*,† Ilya Grinberg, and Andrew M. Rappe

The Makineni Theoretical Laboratories, Department of Chemistry, University of Pennsylvania, Philadelphia, Pennsylvania 19104-6323

Received: July 9, 2007; In Final Form: October 22, 2007

We demonstrate that variations in the molecular chemisorption energy on different metals, different surface terminations, and different strain conditions can be accounted for by orbital-specific changes in the substrate electronic structure. We apply this analysis to a density functional theory data set, spanning three metals, two surface terminations, and five strain states. A crucial aspect of our analysis is decomposition of the d band into contributions from the five d atomic orbitals. This provides a representation of the energy levels of the substrate that are directly relevant to the chemisorption bond, leading to strong correlation with chemisorption trends.

I. Introduction

An important aim of current research is to better understand how surface modification can be used to control surface reactivity.[1−7] The ultimate goal is to be able to apply this comprehension to better surface catalyst design. Due to its relevance to fuel combustion, the treatment of automotive exhaust, and various manufacturing processes, the adsorption of CO on pure and modified surfaces has become the emblematic subject of many experimental and theoretical studies.[8−12] Key advances have established a theoretical understanding of the CO chemisorption bond on metal surfaces. In the Blyholder model,[13] the chemisorption bond is the result of a charge transfer from the substrate into the empty CO $2\pi^*$ orbitals (back-bonding) and direct bonding between the substrate and the filled CO 5σ orbital. Experimentally, Föhlisch et al.[14] used X-ray photoemission spectroscopy to study the π and σ bonding systems in CO/metal chemisorption. Combining second-order perturbation theory and parameters extracted from density functional theory (DFT), Hammer and co-workers[15] developed a simple yet predictive model for top site chemisorption. The Hammer−Morikawa−Nørskov (HMN) model established the energetic center of the density of states projected onto the substrate d bands, or the d-band center (ϵ_d), as a key parameter in predicting chemisorption trends as a function of metal identity. The HMN model expresses the d contribution to the chemisorption bond as

$$E^{\,d}_{\,chem} = -\left[\frac{4fV_\pi^2}{(\epsilon_{2\pi^*} - \epsilon_d)} + 4fS_\pi V_\pi\right] - \left[\frac{2(1-f)V_\sigma^{\,2}}{(\epsilon_d - \epsilon_{5\sigma})} + 2(1+f)S_\sigma V_\sigma\right] \quad (1)$$

where f is the idealized filling of the metal d bands, V_π^2 is the metal−carbon orbital overlap matrix element, S is the overlap value (the symmetry of which is denoted by the subscript), and $\epsilon_{2\pi^*}$ and $\epsilon_{5\sigma}$ are the energies of the renormalized $2\pi^*$ and 5σ orbitals relative to the Fermi level. The π and σ coupling matrix elements are related to linear muffin tin orbital derived values of V_{s-d}^2.[16]

The HMN model reflects reactivity differences as a function of identity through electronic structure (ϵ_d), size (V, S), and filling (f) and is successful in explaining chemisorption trends across the transition-metal series. In subsequent work, it was shown that ϵ_d is also generally predictive of chemisorption trends on different surface terminations and surface strains.[17,18] However, quantitative accuracy (model predictions accurate within 0.1 eV) is still elusive, and for several cases, there is poor or no correlation between ϵ_d and the chemisorption energies. [19−21]

The sound physical basis of the HMN model, and the strong evidence for its general success, has inspired simple modifications to be made for improved accuracy and understanding in particular systems shown to deviate from the original form. For example, for NO adsorption (which occurs preferentially at fcc hollow sites) on pure and alloy transition-metal surfaces, a weighted ϵ_d approach has been developed.[22] A similar approach was also applied to SO_2 chemisorption.[23]

In the present study, we explore correlations between changes in CO chemisorption on transition-metal surfaces and changes in bare surface electronic structure. The basic expectation from the HMN model is that if a tensile strain is applied, then d states on neighboring surface atoms interact less with each other, and this results in a more localized and higher energy ϵ_d. Since lateral stress changes interplanar separations, straining the systems also probes the interplay between in-plane and interplane perturbations to the surface geometry. At different surface terminations, both the symmetry and the number of surface nearest neighbors change. Simultaneous and systematic study of these two structural modifications enhances the understanding of how surface structure is linked to surface reactivity.

II. Methodology

DFT calculations are performed with a generalized gradient approximation (GGA) exchange-correlation functional[24] and norm-conserving optimized pseudopotentials[25] with the designed nonlocal method for metals.[26,27] The Kohn−Sham orbitals are expanded in a plane-wave basis set truncated at 50 Ry. Metallic fillings are treated using the finite temperature method of

* To whom correspondence should be addressed.
† Current Address: National Institute of Standards and Technology, 100 Bureau Drive, Stop 8443, Gaithersburg, MD 20899-8443.

10.1021/jp075355k CCC: $40.75
Published on Web 01/23/2008

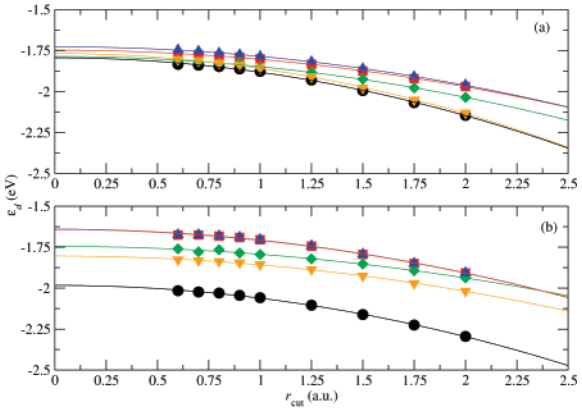

Figure 1. (a) Variation in ϵ_d as a function of projection sphere cutoff radius r_{cut} for Pt(111). $\epsilon_{x^2-y^2}$, ϵ_{xz}, ϵ_{z^2}, ϵ_{yz}, and ϵ_{xy} PDOS centers are shown by black circles, red squares, green diamonds, blue up-triangles, and orange down-triangles, respectively. (b) Same as (a) for Pt(100). The graphs demonstrate the importance of extrapolating $r_{cut} \rightarrow 0$ au. For Pt(111), the asymptotic d-band centers are more nearly equal than their large r_{cut} estimates; for Pt(100), they are more dissimilar.

Mermin[28] with an electronic temperature of 0.2 eV. The zero temperature total energies are estimated by averaging the finite temperature free energy and total energy.[29] DFT calculations are carried out using an in-house code. Pseudopotentials were designed using the OPIUM pseudopotential package.[30] To account for a well-documented DFT−GGA error, [31−33] all CO chemisorption values have been corrected using our first-principles extrapolation procedure.[34] Bare metal surfaces and chemisorption are modeled using slabs of five layers separated by no less than 10.5 Å of vacuum, with the $c(4 \times 2)$ surface cell for (111) surfaces and the $p(2 \times 2)$ surface cell for (100). CO top site and C and O bridge site chemisorption are modeled at a coverage of $\Theta = 0.25$. Calculations are done, and chemisorption energy values are tested to be converged within 0.02 eV, using an $8 \times 8 \times 1$ grid of Monkhorst−Pack k-points,[35] reduced by symmetry where possible.

We have compiled a database of DFT molecular top site (E_{chem}) and dissociative bridge site (E_{dissoc}) chemisorption energies and electronic structure measurements for CO on Pt, Pd, and Rh (111) and (100) surfaces. E_{chem} and E_{dissoc} are determined for each surface at the preferred theoretical lattice constants (3.90, 3.86, and 3.76 Å for Pt, Pd, and Rh, respectively) as well as under in-plane strains of ±1 and ±2%, a range easily achievable through epitaxial mismatch.[36]

For each metal, surface, and strain state, two values for E_{chem} are determined, E_{chem}^{fix} and E_{chem}^{rlx}. The former is the energy gain when the same chemisorption geometry is fixed over the relaxed bare surface for all metals and surfaces. In the latter, full ionic relaxation is allowed in the top two metal surface layers and all C and O ionic degrees of freedom. The advantage to considering the less-realistic E_{chem}^{fix} is to eliminate any variation (as a function of metal, strain, and facet) in adsorption-induced surface relaxation. For the dissociative systems, we only determine E_{dissoc}^{fix} due to the known instability of C and O atomic adsorption at bridge sites.[37]

We focus attention on top site E_{chem} and bridge site E_{dissoc} for clarity. The symmetries at these sites provide for zero overlap between some d orbitals and the adsorbate orbitals. Explicitly, in a top site geometry, d_{z^2} is the only metal atomic d orbital that has nonzero overlap with the CO 5σ molecular orbital. The d_{xz} and d_{yz} are the only atomic metal orbitals to have nonzero overlap with the CO $2\pi^*$ orbitals, and the overlap between $2\pi_x^*$ and d_{xz} is equal to the overlap between $2\pi_y^*$ and d_{yz}. This

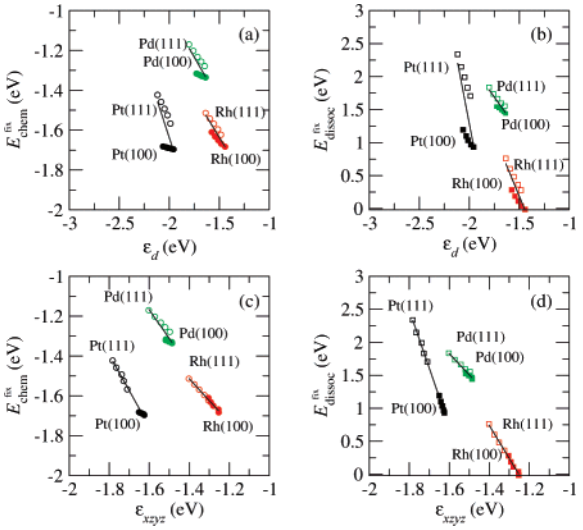

Figure 2. Plots of E_{chem}^{fix} and E_{dissoc}^{fix} versus ϵ_d and ϵ_{xzyz} for Pt (circle), Rh (square), and Pd (diamond) (111) surfaces (open) and (100) surfaces (filled). Data for five lateral strain states (0, ±1, and ±2%) are shown. Linear regressions are shown for each metal. (a) E_{chem}^{fix} versus ϵ_d; $r_{cut} = 2$ au. (b) E_{dissoc}^{fix} versus ϵ_d; $r_{cut} = 2$ au. (c) E_{chem}^{fix} versus ϵ_{xzyz}; $r_{cut} \rightarrow 0$ au. (d) E_{dissoc}^{fix} versus ϵ_d and ϵ_{xzyz}; $r_{cut} \rightarrow 0$ au.

indicates that the entire direct bonding contribution to E_{chem} depends on the d_{z^2} contribution to the projected density of states (PDOS), while the back-bonding contribution depends on the $d_{(xz+yz)/2}$ contribution. For late series transition metals, eq 1 indicates that the back-bonding contribution to the chemisorption bond will be dominant, and we therefore focus on the π contribution to CO chemisorption. The bridge site atomic adsorption geometry is also dominated by d_{xz} and d_{yz} states. These bonding geometries therefore lend themselves readily to symmetry-specific analysis of the substrate d band. These geometries are also ideal for consideration in that, while the substrate−substrate overlap varies with changes in the in-plane lattice constant and surface termination, the substrate−adsorbate overlap does not change to an appreciable extent. This allows us to make direct comparisons of strain effects on different facets. For each metal studied, we observe no appreciable variation in the value of f for the range of strain and different terminations considered here. This indicates that V, S, and f can be viewed as constant under the range of surface geometries studied for each metal, and therefore, the full extent of variation in E_{chem} for each metal should be traceable to variations in the surface electronic structure. However, even at low-symmetry sites, the contributions of the five d orbitals to chemisorption are unequal, making treatment of individual d orbitals more accurate in general.

The projected density of states (PDOS) for each orbital is constructed by projecting each atomic valence pseudo-wave function (radial wave function multiplied by a real combination of spherical harmonics) of the surface atoms onto all of the Kohn−Sham orbitals. Values of ϵ_d are then calculated as the first moment of each PDOS.

To reduce PDOS contributions from neighboring surface atoms, projection is performed within a sphere of radius r_{cut} centered about the surface atom of interest. Standard practice is to use a constant value for r_{cut} when comparing the PDOS and associated ϵ_d values of different surfaces, and $r_{cut} = 2$ au is the default in some widely used DFT packages. [38−40] However, this approach leaves significant contributions from the orbitals of other atoms, making the calculated value of ϵ_d dependent on r_{cut}, which is undesirable.

TABLE 1: E^{fix}_{chem}, E^{rlx}_{chem}, E^{fix}_{dissoc}, ϵ_d, and ϵ_{xzyz} in eV for the (111) and (100) Surfaces of Pt, Rh, and Pd. The Slope of Each Quantity with Respect to In-Plane Strain (d/ds) is Also Reported in Units of meV/% Strain (ϵ_d and ϵ_{xzyz} use $r_{cut} \rightarrow 0$ au)

	Efix $_{chem}$	(dE/ds)	E^{rlx}_{chem}	(dE/ds)	E^{fix}_{dissoc}	(dE/ds)	ϵ_d	(dϵ/ds)	ϵ_{xzyz}	(dϵ/ds)
Pt(111)	−1.49	−36	−1.58	−46	1.99	−158	−1.77	20	−1.74	18
Pt(100)	−1.69	−3	−1.81	−5	1.03	−65	−1.76	20	−1.63	7
Rh(111)	−1.56	−27	−1.68	−24	0.48	−120	−1.38	31	−1.35	25
Rh(100)	−1.65	−18	−1.74	−9	0.11	−74	−1.36	29	−1.28	14
Pd(111)	−1.23	−25	−1.26	−29	1.66	−70	−1.58	32	−1.54	26
Pd(100)	−1.32	−5	−1.36	−6	1.50	−29	−1.56	19	−1.50	9

To eliminate contamination from the orbitals of neighboring atoms, we evaluated ϵ_d at various r_{cut} values. (When $r_{cut} < 0.5$ au, the number of FFT grid points is too small to allow spherical sampling; therefore, data are presented for $r_{cut} \geq 0.6$ au.) Figure 1 shows the variation of ϵ_d with r_{cut} for Pt(111) and Pt(100). It is apparent that the asymptotic behavior of ϵ_d is not reached until $r_{cut} \ll 2$ au. Furthermore, ϵ_d values for different surfaces, strain states, and orbital angular momenta depend differently on r_{cut}. To obtain accurate ϵ_d values, we fit a purely quadratic function to the data and extrapolate ϵ_d to $r_{cut} = 0$. This procedure greatly reduces the contribution from the orbitals of neighboring atoms, making comparison of ϵ_d for various systems more meaningful.

In our examination of the strain impact on chemisorption, we focus on the changes induced by facet and strain to the electronic structure of the metal. This is due to the lack of contribution from the interadsorbate interactions to the differences in the response of CO E_{chem} to strain on the (111) and the (100) surfaces. This can be shown by examination of CO−CO repulsive interactions at the distances relevant to our study.

In previous work, our DFT calculations found that the energy cost due to repulsive interaction between CO molecules at the $\sqrt{3/2}a$ and $\sqrt{2}a$ interadsorbate separations present, respectively, in our $c(4 \times 2)$ (111) surface supercells and $p(2 \times 2)$ (100) surfaces supercells are, at most, a few meV.[10] For both surfaces, the strain slopes found by our calculations are much larger than those expected from interadsorbate interactions, and it is therefore the electronic structure of the surface that is responsible for the variation in chemisorption energy induced by strain and facet changes. Similar arguments also hold for the atomic adsorption on the bridge site, eliminating interadsorbate interactions as the main cause of the differences in E_{dissoc} dependence on strain.

All of the CO E_{chem} values reported in Table 1 have been treated with our post-DFT extrapolation procedure.[34] We have previously established the applicability of this method to a variety of metals, surfaces, and varying CO densities.[10] There are subtle variations in the corrections to E_{chem} between the (111) and (100) surface terminations of each metal.[34] Test calculations showed that the corrections to E_{chem} do not appreciably evolve under the 2% range of in-plane strain on either termination or in going from E^{rlx}_{chem} to E^{fix}_{chem}. The resulting effect of the correction on the tabulated data is that all uncorrected values of E_{chem} are higher (meaning more strongly bound) by 0.120 eV on Pt(111) and Pt(100), by 0.104 eV on Pd(111), by 0.110 eV on Pd(100), by 0.162 eV on Rh(111), and by 0.138 eV on Rh(100). Our use of highly accurate, corrected E_{chem} values eliminates the possible contribution of the known DFT−GGA E_{chem} overestimation to changes in E_{chem} with strain and facet change. Therefore, the variations in E_{chem} values obtained by us for different strain states and surface terminations are entirely due to variations in the surface electronic structure.

III. Results

The results for E_{chem} are presented in Table 1. Inspection of the data shows that chemisorption on the (100) facet is stronger than that on the (111) facet for all metals. This facet effect is notably dependent on the metal identity. On Pt, $E^{rlx,100}_{chem} - E^{rlx,111}_{chem}$ is 0.23 eV, or about 14.5% of $E^{rlx,111}_{chem}$. For Rh, the increase is only 0.06 eV, or about 3.6% of $E^{rlx,111}_{chem}$. As the substrate is strained to increase the effective lateral lattice constant, E_{chem} increases for all metals and on both facets. However, the extent of the strain effect is different depending on the facet and is much greater on the (111) facet than on the (100) facet.

While examination of the relationship between E_{chem} and ϵ_d (Figure 2) shows that E_{chem} qualitatively tracks with ϵ_d for the (111) surfaces, it also reveals shortcomings of using ϵ_d for modeling bonding on different facets. From Figure 2, we see that E_{chem} values on different facets differ by 0.06−0.25 eV (0.15−0.85 eV for E_{dissoc}), even though they have the same ϵ_d and the same metal. Figure 2 and Table 1 show that this is still true for ϵ_d with $r_{cut} \rightarrow 0$ au. Therefore, neither E^{fix}_{chem} nor E^{fix}_{dissoc} can be fit as a single function of ϵ_d when both (111) and (100) facets are considered.

By contrast, we find that facet dependence of the chemisorption energies can be fit as a single linear function of ϵ_{xzyz}, the band center of the d_{xz} and d_{yz} orbitals. Figure 2 shows that single linear regressions of data for both facets are accurate to within 0.05 eV in all cases. This result demonstrates that focusing on the metal orbitals involved in bonding simplifies the observed chemisorption behavior.

Similarly, Table 1 shows that the response of E_{chem} and E_{dissoc} to strain is reflected in ϵ_{xzyz} but not in ϵ_d. The tunability of E_{chem} and E_{dissoc} through strain is 2−10 times greater on the (111) surfaces. However, dϵ_d/ds is identical within computational precision for the two facets of Pt and Rh. In contrast, the chemisorption tunability trend is strongly reflected in dϵ_{xzyz}/ds due to the key role that the d_{xz} and d_{yz} orbitals play in top site molecular and bridge site dissociative adsorption of CO.

We now explain the differences in E_{chem} trends on (111) and (100) facets of the same metal in terms of substrate electronic structure. First, we consider the salient electronic structure differences between the (111) and (100) surface facets. The dd metal bonding can be decomposed by symmetry into σ, π, and δ contributions.[41] The square lattice of the (100) surface allows for strong ddσ overlap between neighboring $d_{x^2-y^2}$ orbitals. This lowers the energy of the $d_{x^2-y^2}$ states on the (100) surface relative to that on the (111) surface, as shown by our DFT calculations of $\epsilon_{x^2-y^2}$ (Figures 1 and 3). In contrast to the $d_{x^2-y^2}$ orbitals, the d_{xz} and d_{yz} states are significantly *higher* in energy on (100) than on (111), as shown in Figure 3. This is partially due to the difference in surface geometry and partially due to the smaller number of nearest neighbors on the (100) surface. The rise in ϵ_{xz} and ϵ_{yz} gives rise to stronger chemisorption on the (100) surface. Averaging all of the d orbitals causes the rise in

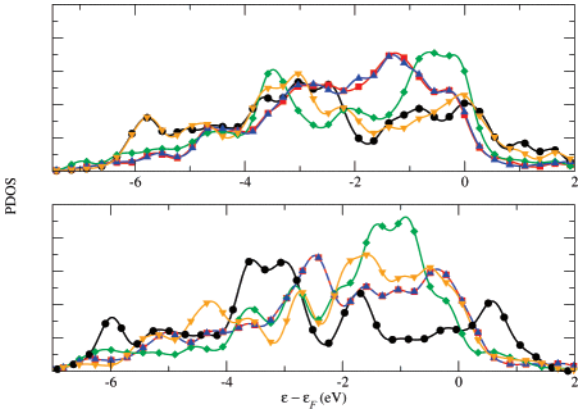

Figure 3. (a) PDOS for each d state of Pt(111). $\epsilon_{x^2-y^2}$, ϵ_{xz}, ϵ_{z^2}, ϵ_{yz}, and ϵ_{xy} PDOS's are shown in black, red, green, blue, and orange, respectively. (b) Same as (a) for Pt(100). Data PDOS calculations with $r_{cut} = 2.0$ au were used. Gaussian smearing has been applied to the discrete output.

bonding-relevant ϵ_{xz} and ϵ_{yz} to be masked by the drop in bonding-irrelevant $\epsilon_{x^2-y^2}$, so that even though ϵ_{xzyz} closely tracks the increase in E_{chem} on the (100) surface relative to the (111) surface, the averaged ϵ_d does not.

The effects of strain on the d orbitals are also dependent on their orientations relative to the surface, and this leads to differences in the strain response of E_{chem} on the (111) and (100) facets. The interplanar spacing between the top two metal layers (r_{12}) responds to the strain; approximate conservation of volume suggests that tensile lateral strain decreases r_{12}, while compression increases r_{12}. The bonding-relevant d_{xz} and d_{yz} orbitals of the top layer have the strongest interaction with the second layer atoms; therefore, the relaxation of r_{12} significantly reduces the effect of lateral strain for these orbitals. This is why $d\epsilon_{xzyz}/ds$ is less than $d\epsilon_d/ds$ for all surfaces studied (Table 1). The effect of r_{12} relaxation on strain tunability is also strongly facet-dependent. On the more open (100) surface, relaxations of r_{12} are larger, making $d\epsilon_{xzyz}/ds$ smaller for each (100) facet studied than that for the corresponding (111) facet. This explains why the tunability of E_{chem} (fix and rlx) and E_{dissoc}^{fix} are much lower on (100) surfaces than those on (111) surfaces.

IV. Conclusions

We have presented an orbital-specific analysis of CO chemisorption as a function of metal identity, facet, and strain state. Chemisorption trends are better described through orbital-specific modeling than through total average substrate electronic properties. We have also shown that trends in the dissociative chemisorption of CO at the bridge site are governed by the same orbital-specific factors. The orbital-specific analysis presented is applicable to a broader range of chemisorption systems. DFT studies have found that reactions on late transition metals usually proceed on defects such as steps and kinks.[42] The analysis presented here suggests that for such low-symmetry sites, the electronic structure parameters relevant for bonding may be significantly different from the average d-band center, necessitating orbital-specific modeling to explain chemisorption properties.

Acknowledgment. This work was supported by the Air Force Office of Scientific Research, Air Force Materiel Command, USAF, under Grant No. FA9550-07-1-0397 and by the Department of Energy Office of Basic Energy Sciences under Grant No. DE-FG02-07ER15920. Computational support was provided by a Challenge Grant from the High-Performance Computing Modernization Office of the Department of Defense.

References and Notes

(1) Gsell, M.; Jakob, P.; Menzel, D. *Science* **1998**, *280*, 717.
(2) Rose, M. K.; Mitsui, T.; Dunphy, J.; Borg, A.; Ogletree, D. F.; Salmeron, M.; Sautet, P. *Surf. Sci.* **2002**, *512*, 48.
(3) Schlapka, A.; Lischka, M.; Gross, A.; Käsberger, U.; Jakob, P. *Phys. Rev. Lett.* **2003**, *91*, 016101.
(4) Kitchin, J. R.; Nørskov, J. K.; Barteau, M. A.; Chen, J. G. *Phys. Rev. Lett.* **2004**, *93*, 156801.
(5) Tsuda, M.; Kasai, H. *Phys. Rev. B* **2006**, *73*, 155405.
(6) Grabow, L.; Xu, Y.; Mavrikakis, M. *Phys. Chem. Chem. Phys.* **2006**, *8*, 3369.
(7) Nilekar, A. U.; Greeley, J.; Mavrikakis, M. *Angew. Chem., Int. Ed.* **2006**, *45*, 7046.
(8) Koper, M. T. M.; van Santen, R. A.; Wasileski, S. A.; Weaver, M. J. *J. Chem. Phys.* **2000**, *113*, 4392.
(9) Neef, M.; Doll, K. *Surf. Sci.* **2006**, *600*, 1085.
(10) Mason, S. E.; Grinberg, I.; Rappe, A. M. *J. Phys. Chem. B* **2006**, *110*, 3816.
(11) Dupont, C.; Jugnet, Y.; Loffreda, D. *J. Am. Chem. Soc.* **2006**, *128*, 9129.
(12) Vermang, B.; Jeul, M.; Raaen, S. *Phys. Rev. B* **2006**, *73*, 033407.
(13) Blyholder, G. *J. Phys. Chem.* **1964**, *68*, 2772.
(14) Föhlisch, A.; Nyberg, M.; Hasselström, J.; Karis, O.; Pettersson, L. G. M.; Nilsson, A. *Phys. Rev. Lett.* **2000**, *85*, 3309.
(15) Hammer, B.; Morikawa, Y.; Nørskov, J. K. *Phys. Rev. Lett.* **1996**, *76*, 2141.
(16) Ruban, A.; Hammer, B.; Stoltze, P.; Skriver, H. L.; Nørskov, J. K. *J. Mol. Catal. A: Chem.* **1997**, *115*, 421.
(17) Hammer, B.; Nielsen, O. H.; Nørskov, J. K. *Catal. Lett.* **1997**, *46*, 31.
(18) Mavrikakis, M.; Hammer, B.; Nørskov, J. K. *Phys. Rev. Lett.* **1998**, *81*, 2819.
(19) Lu, C.; Lee, I. C.; Masel, R. I.; Wieckowski, A.; Rice, C. *J. Phys. Chem. A* **2002**, *106*, 3084.
(20) Liu, Z. P.; Stephen, J. J.; King, D. A. *J. Am. Chem. Soc.* **2004**, *126*, 10746.
(21) Cooper, V. R.; Kolpak, A. M.; Yourdshahyan, Y.; Rappe, A. M. *Phys. Rev. B Rapid Commun.* **2005**, *72*, 081409(R).
(22) Tang, H.; Trout, B. L. *J. Phys. Chem. B* **2005**, *109*, 17630.
(23) Tang, H.; Trout, B. L. *J. Phys. Chem. B* **2005**, *109*, 6948.
(24) Perdew, J. P.; Burke, K.; Ernzerhof, M. *Phys. Rev. Lett.* **1996**, *77*, 3865.
(25) Rappe, A. M.; Rabe, K. M.; Kaxiras, E.; Joannopoulos, J. D. *Phys. Rev. B Rapid Commun.* **1990**, *41*, 1227.
(26) Ramer, N. J.; Rappe, A. M. *Phys. Rev. B* **1999**, *59*, 12471.
(27) Grinberg, I.; Ramer, N. J.; Rappe, A. M. *Phys. Rev. B Rapid Commun.* **2001**, *63*, 201102(R).
(28) Mermin, N. D. *Phys. Rev. A* **1965**, *137*, 1441.
(29) Vita, A. D.; Gillan, M. J. *J. Phys.: Condens. Matter* **1991**, *3*, 6225.
(30) Opium: Pseudopotential Generation Project. http://opium.sourceforge.net (2007).
(31) Feibelman, P. J.; Hammer, B.; Nørskov, J. K.; Wagner, F.; Scheffer, M.; Stumpf, R.; Watwe, R.; Dumesic, J. *J. Phys. Chem. B* **2001**, *105*, 4018.
(32) Grinberg, I.; Yourdshahyan, Y.; Rappe, A. M. *J. Chem. Phys.* **2002**, *117*, 2264.
(33) Hu, Q. M.; Reuter, K.; Scheffer, M. *Phys. Rev. Lett.* **2007**, *98*, 176103.
(34) Mason, S. E.; Grinberg, I.; Rappe, A. M. *Phys. Rev. B* **2004**, *69*, 161401(R).
(35) Monkhorst, H. J.; Pack, J. D. *Phys. Rev. B* **1976**, *13*, 5188.
(36) Hrbek, J.; Hwang, R. Q. *Curr. Opin. Solid State Mater. Sci.* **2001**, *5*, 67.
(37) Ford, D. C.; Xu, Y.; Mavrikakis, M. *Surf. Sci.* **2005**, *587*, 159.
(38) Gonze, X.; Beuken, J.-M.; Caracas, R.; Detraux, F.; Fuchs, M.; Rignanese, G. M.; Sindic, L.; Verstraete, M.; Zerah, G.; Jollet, F.; Torrent, M.; Roy, A.; Mikami, M.; Ghosez, P.; Raty, J. Y.; Allan, D. C. *Comput. Mater. Sci.* **2002**, *25*, 478.
(39) ABINIT Homepage. http://www.abinit.org/.
(40) Dacapo. http://dcwww.camp.dtu.dk/campos/Dacapo/.
(41) Sutton, A. P. *Electronic Structure of Materials*; Oxford University Press: New York, 1993.
(42) Liu, Z.-P.; Hu, P. *J. Am. Chem. Soc.* **2003**, *125*, 1958.